

SOME EXTENSIONS TO DIRECT SIMULATION CALCULATIONS OF RAREFIED HYPERSONIC GAP FLOW

Luis T. L. C. Paolicchi, lucchi@lep.inpe.br

Wilson F. N. Santos, wilson@lep.inpe.br

National Institute for Space Research, Combustion and Propulsion Laboratory, Cachoeira Paulista-SP, 12630-000 BRAZIL

Abstract. Numerical simulations of two-dimensional rarefied hypersonic flow in a family of gap are performed by using the Direct Simulation Monte Carlo (DSMC) method. The work focuses on the length-to-depth (L/H) ratio effects on the flowfield structure. The length L and the depth H were changed in a such way that the L/H ratio was kept to $1/4$. Numerical results of flow characteristics, including the streamlines, and velocity, density, temperature and viscosity profiles, are presented for three different gap length and depth. The analysis showed significant differences in the flow topology for a gap in the transition flow regime. For the conditions investigated, it was found only one vortex core instead of a column of vortices usually observed inside the gaps in the continuum flow regime.

Keywords: DSMC, Hypersonic Flow, Rarefield Flow, Gap.

1. INTRODUCTION

Separated and/or reattached supersonic/hypersonic flows have received considerable attention in the last decades. This growing interest is intimately connected with their frequent occurrence on the surfaces of high-speed aerodynamic structures. Many problems of physical interest involve separation and/or reattachment flows, which can occur in a variety of ways. For instance, the maximum lift of an airfoil is limited by the occurrence of separation. Separated regions can also occur in an overexpanded rocket nozzle, behind a blunt base, on the leeward side of an object inclined at large angle of attack, or by an oblique shock wave incident on the boundary layer.

An interesting class of problems involving separated and/or reattached flows arises when discontinuities or imperfections, such as protuberances, notches, steps, cavities or gaps, are present on the surface of reentry hypersonic vehicles. The presence of these discontinuities or imperfections in modern aerodynamics configurations occurs as a desired or undesired design feature. As an illustrative example, the thermal protection system (TPS) of the experimental Crew Rescue Vehicle X-38 requires gaps between the TPS tiles, as displayed in Fig. 1(a). Similarly, a large part of the TPS of the Space Shuttle Orbiter consists of reusable surface insulation tiles, as illustrated in Figs. 1(b-d). Gaps between the tiles are necessary in order to account for the thermal expansion of the structure to which the TPS tiles are attached. Usually, the majority of the TPS tiles consists of silica foam with 6 x 6 inches square, with variable depth that depends on the tile location on the Orbiter. In principle, the flow is very complex in the gaps between tiles, since hot gases may flow into the gaps and cause an increase in the heating rate to the tile sidewall and the underlying aluminum structure (Scott and Maraia, 1979).

A large amount of research studies have already been conducted to investigate the flowfield structure on gaps (Bertin and Goodrich, 1980; Everhart *et al.*, 2006; Hinderks *et al.*, 2004; Hinderks and Radespiel, 2006; Petley *et al.*, 1984; Pitts and Murbach, 1982; Scott and Maraia, 1979; Smith *et al.*, 1983; Vharbonnier and Boerrigter, 1993). For the purpose of this introduction, it will be sufficient to describe only a few of these studies.

Scott and Maraia (1979) have investigated the heating rate distribution and the temperature response on the gap walls of protection tiles. The analysis showed that the hottest location measured in the gap was at 0.75 inch from the upstream transverse gap, and the heat flux distribution in the gap was not constant in time, since the convective heating rate depended on the wall temperature of the gap. In addition, they have demonstrated that the heating rate depended on the gap width.

Hinderks *et al.* (2004) have investigated the gap flow structure. They showed that exist a complex flow within the gap, consisting of an vortex superposed by an axial flow. The analysis showed that the heat flux transferred to the structure depends on the thermal state of the structure. Also, effects due to changes in the gap geometry caused by deformations in the gap structure demonstrated that deformations should be considered in the design analysis.

The extensive literature on gaps is devoted primarily to laminar or turbulent flow over a wide range of Mach numbers in the continuum flow regime. However, there is little understanding of the physical aspects of hypersonic flow past to gaps related to the severe aerothermodynamic environment associated to a reentry vehicle.

In this context, Paolicchi and Santos (2009) have studied gaps situated in a rarefied hypersonic flow by employing the DSMC method. The work was motivated by the interest in investigating the length-to-depth (L/H) ratio effects on the flowfield structure. The primary emphasis was to examine the behavior of the primary properties, such as velocity, density, pressure and temperature, due to variations on the gap L/H ratio from 1 to $1/4$. The analysis showed that the gap flow behavior in the transition flow regime differs from that found in the continuum flow regime. It was found only one vortex core for the L/H ratio investigated, in contrast to the vortices expected for the continuum flow regime, which is given approximately by H/L ratio.

In continuation of the gap research, Paolicchi and Santos (2010) extended the previous analysis (Paolicchi and Santos,

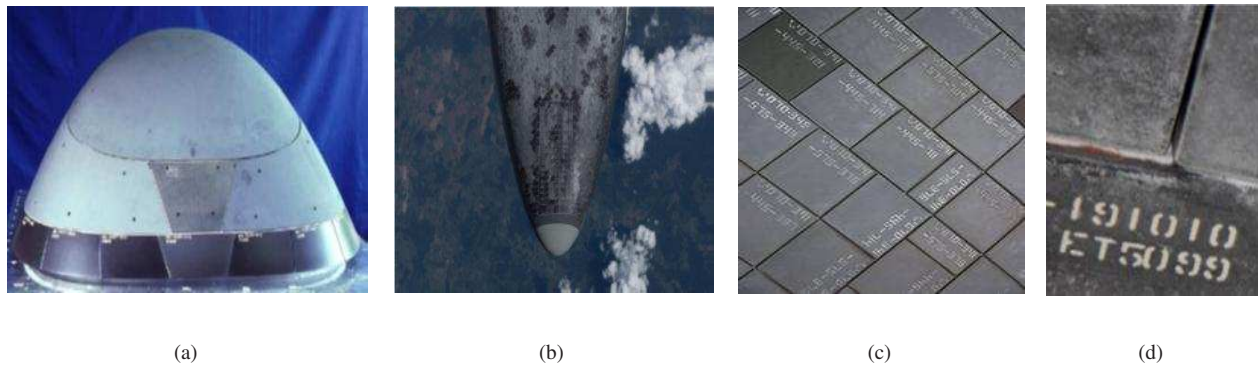


Figure 1. Drawings illustrating the (a) X-38 nose cap, the (b) space shuttle tiles, (c) a magnified view of the space shuttle tiles, and (d) a magnified view of a gap.

2009) by investigating the effects of the gap L/H ratio on the aerodynamic surface quantities. In this manner, the investigation was undertaken in an attempt to assess the behavior of the heat transfer, pressure, and skin friction coefficients due to changes on the gap L/H ratio. The analysis showed that the heat flux and pressure loads depend on the L/H ratio. It was found that the peak values for the heat transfer coefficient took place on the gap forward face, and they were twice of the maximum value observed for a smooth surface, i.e., a flat plate without a gap. A similar behavior was found for the pressure loads. The peak value for the pressure coefficient also occurred at the gap forward face, and it was around 3.8 times larger than the peak value for a smooth surface.

The current study expands on the results presented in the previous analysis (Paolicchi and Santos, 2009) in order to provide a comprehensive description of the flowfield structure inside the gaps with special relevance to the recirculation region. In this scenario, the present investigation was undertaken in an attempt to gain some insight into the physics of the vortex formation in the gaps for a flow in the transition flow regime, i.e., between the continuum flow and the free molecular flow.

2. FLOWFIELD STRUCTURE

According to the literature (Everhart *et al.*, 2006), length-to-depth (L/H) ratio is used to classify cavity flow physics. Short or deep cavities defined by $L/H < 1$ are the important class of cavities known as gaps. Usually, in the continuum flow regime, the gap flow topology is defined by the development of a column of counter-rotating vortices within the gap caused by the main stream flow, where the number of vortices is approximately given by H/L . In addition, alternating hot spots are developed in the gap when the vortices directionally align and impinge on the gap sidewall. Figure 2(a) exhibits a schematic view of the flow topology inside a gap.

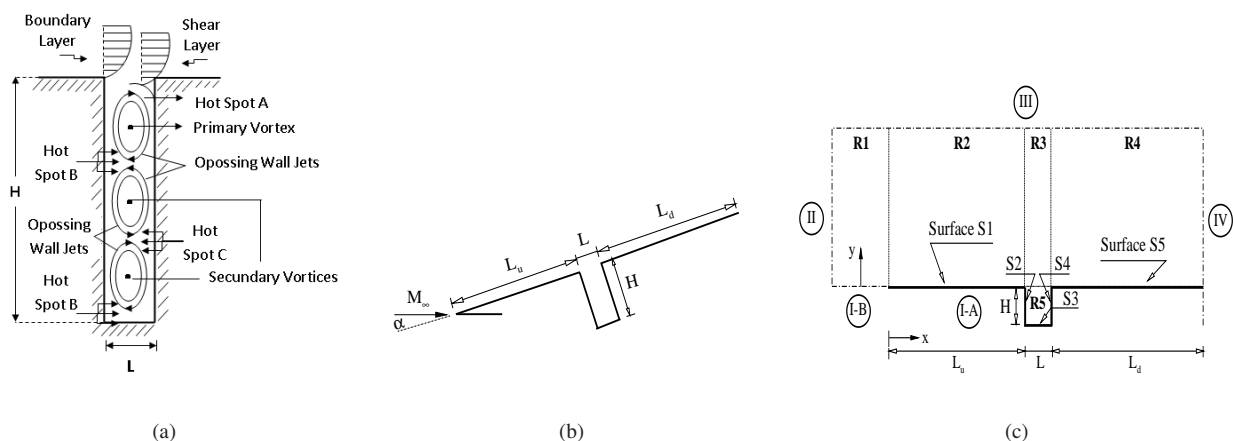


Figure 2. Drawings illustrating the (a) flow topology inside a gap, (b) a schematic view of the gap configuration, and (c) the computational domain.

3. GEOMETRY DEFINITION

In the present work, discontinuities in a reentry capsule surface is modeled by a gap, length L and depth H , as defined in the previous work, Paolicchi and Santos (2009). By considering that the depth H is much smaller than the nose radius R of a reentry capsule (for instance, similar to that one shown in Fig. 1(a)), i.e., $H/R \ll 1$, then the hypersonic flow over the gap may be considered as a hypersonic flow over a flat plate with a gap. Figure 2(b) illustrates a schematic view of the model employed.

Referring to Fig. 2(b), α stands for the angle of attack, M_∞ represents the freestream Mach number, H the gap depth, L the gap length, L_u the length of the gap upstream surface, and L_d the length of the gap downstream surface. It was assumed a length L of 3, 4, and 5 mm, and a depth H of 3, 6, 9, 12, 16, and 20 mm. In addition, L_u/λ_∞ of 50 and L_d/λ_∞ of 50, where λ_∞ is the freestream mean free path. It was considered that the flat plate is infinitely long but only the total length $L_u + L + L_d$ is investigated.

4. FREESTREAM AND FLOW CONDITIONS

Freestream and flow conditions used for the numerical simulations are those given by Paolicchi and Santos (2009) and summarized in Tab. (1), and the gas properties (Bird, 1994) are shown in Tab. (2).

Table 1. Freestream flow conditions

Altitude (km)	T_∞ (K)	p_∞ (N/m ²)	ρ_∞ (kg/m ³)	μ_∞ (Ns/m ²)	n_∞ (m ⁻³)	λ_∞ (m)
70	219.69	5.582	8.753×10^{-5}	1.455×10^{-5}	1.8192×10^{21}	9.285×10^{-4}

The freestream velocity U_∞ is assumed to be constant at 7456 m/s, which corresponds to a freestream Mach number M_∞ of 25. The wall temperature T_w is assumed constant at 880 K. This temperature is chosen to be representative of the surface temperature near the stagnation point of a reentry capsule and is assumed to be uniform over the gap surface. It is important to mention that the surface temperature is low compared to the stagnation temperature of the air. This assumption seems reasonable since practical surface material will probably be destroyed if surface temperature is allowed to approach the stagnation temperature.

Table 2. Gas properties

	X	m (kg)	d (m)	ω
O_2	0.237	5.312×10^{-26}	4.01×10^{-10}	0.77
N_2	0.763	4.650×10^{-26}	4.11×10^{-10}	0.74

By assuming the gap depth H as the characteristic length, the Knudsen number Kn_H corresponds to the range from 0.3095 to 0.0464 for depth H from 3 to 20 mm, respectively. Finally, the Reynolds number Re_H is from 121.7 to 811.3 for depth H from 3 to 20 mm, respectively, also based on conditions in the undisturbed stream. Finally, it was assumed a zero-degree angle of attack. It is important to remark that the simulations covered two group of L/H ratio; the first one, from 1 to 1/4, which correspond to the gap length L of 3 mm and gap depth H of 3, 6, 9, and 12 mm, and the second one, for a fixed $L/H = 1/4$, which correspond to gap length L of 3, 4, and 5 mm with gap depth H of 12, 16 and 20 mm, respectively.

5. COMPUTATIONAL METHOD

The Direct Simulation Monte Carlo (DSMC) method (Bird, 1994) is a computational technique for modeling complex transitional flows of engineering interest. The DSMC method model a gas flow by using a computer to track the trajectory of simulated particles, where each simulated particle represents a fixed number of real gas particles. The direct simulation of the physical processes is in contrast with computation fluid dynamics (CFD) method that is applied to the mathematical equations that model the physical processes. The uncoupling of the molecular motion and collisions over small time steps and the division of the flowfield into small cells are the key computational assumptions associated with the DSMC method. The method has been tested in the transition flow regime in the last 50 years, and has shown excellent results when compared with experimental data (Harvey, 1986; Harvey and Gallis, 2000, 2003; Holden and Wadhams, 2003).

Collisions in the present DSMC code are simulated with the variable hard sphere (VHS) molecular model (Bird, 1981) and the no time counter (NTC) collision sampling technique (Bird, 1989). Energy exchange between kinetic and internal modes is controlled by the Borgnakke-Larsen statistical model (Borgnakke and Larsen, 1975). For the present account, the simulations are performed using a non-reacting gas model, consisting of 76.3% of N_2 and 23.7% of O_2 , while considering energy exchange between translational, rotational and vibrational modes. For a given collision, the probability is defined by the inverse of the number of relaxation, which corresponds to the number of collisions needed, on average, for a

molecule undergoes relaxation. The probability of an inelastic collision determines the rate at which energy is transferred between the translational and internal modes after an inelastic collision. Relaxation collision numbers of 5 and 50 were used for the calculations of rotation and vibration, respectively.

6. COMPUTATIONAL FLOW DOMAIN AND GRID

For the numerical treatment of the problem, the computational domain used for the calculation is made large enough so that gap disturbances do not reach the upstream and side boundaries, where freestream conditions are specified. A schematic view of the computational domain is depicted in Fig. 2(c). The computational domain is divided into five regions (R1 to R5), which are subdivided into computational cells. The cells are further subdivided into subcells, two subcells/cell in each coordinate direction. The cell provides a convenient reference for the sampling of the macroscopic gas properties, while the collision partners are selected from the same subcell for the establishment of the collision rate.

According to Fig. 2(c), side I-A is defined by the gap surface. Diffuse reflection with complete thermal accommodation is the condition applied to this side. In a diffuse reflection, the molecules are reflected equally in all directions, and the final velocity of the molecules is randomly assigned according to a half-range Maxwellian distribution determined by the wall temperature. Side I-B is a plane of symmetry, where all flow gradients normal to the plane are zero. At the molecular level, this plane is equivalent to a specular reflecting boundary. Side II is positioned at $5\lambda_\infty$ upstream of the flat-plate leading edge, and side III defined at $25\lambda_\infty$ above the flat plate. Finally, the flow at the downstream outflow boundary, side IV, is predominantly supersonic and vacuum condition is specified (Bird, 1994). At this boundary, simulated molecules can only exit.

The numerical accuracy in DSMC method depends on the cell size chosen, on the time step as well as on the number of particles per computational cell. In the DSMC code, the linear dimensions of the cells should be small in comparison with the scale length of the macroscopic flow gradients normal to the streamwise directions, which means that the cell dimensions should be of the order of or smaller than the local mean free path (Alexander *et al.*, 1998, 2000). The time step should be chosen to be sufficiently small in comparison with the local mean collision time (Garcia and Wagner, 2000; Hadjiconstantinou, 2000). In general, the total simulation time, discretized into time steps, is identified with the physical time of the real flow. Finally, the number of simulated particles has to be large enough to make statistical correlations between particles insignificant.

These effects were investigated in order to determine the number of cells and the number of particles required to achieve grid independence solutions. A grid independence study was made with three different structured meshes – coarse, standard and fine – in each coordinate direction. The effect of altering the cell size in the x - and y -directions was investigated for a coarse and fine grids with, respectively, 50% less and 100% more cells with respect to the standard grid. In addition, each grid was made up of non-uniform cell spacing in both directions. Moreover, point clustering is used close to solid walls and to the horizontal plane connecting the two corners. Table 3 tabulates the number of cells employed in the four regions for coarse, standard, and fine grids for the $L/H = 1$ case.

The effect (not shown) of changing the cell size in both directions on the heat transfer, pressure and skin friction coefficients was rather insensitive to the range of cell spacing considered, indicating that the standard grid, with a total of 15,000 cells, for the $L/H = 1$ case, is essentially grid independent.

A similar examination was made for the number of molecules. The standard grid for the $L/H = 1$ case corresponds to, on average, a total of 314,700 molecules. Two new cases using the same grid were investigated. These two new cases correspond to 157,500 and 630,600 molecules in the entire computational domain. As the three cases presented the same results (not shown) for the heat transfer, pressure and skin friction coefficients, hence the standard grid with a total of 314,700 molecules is considered enough for the computation of the flowfield properties. A complete discussion of the verification and validation processes is described in detail in Paolicchi (2010).

Table 3. Number of cells in the (x -direction investigation) and [y -direction investigation] for the $L/H = 1$ case.

	Region 1	Region 2	Region 3	Region 4	Region 5	Total number of cells
Coarse	(5 × 40)	(60 × 50)	(10 × 50)	(60 × 60)	(10 × 10)	7,500
	[10 × 20]	[120 × 25]	[20 × 25]	[120 × 30]	(20 × 10)	30,000
Standard	10 × 40	120 × 50	20 × 50	120 × 60	(20 × 20)	15,000
Fine	(20 × 40)	(240 × 50)	(40 × 50)	(240 × 60)	(40 × 20)	7,500
	[10 × 80]	[120 × 100]	[20 × 100]	[120 × 120]	(20 × 40)	30,000

7. COMPUTATIONAL RESULTS AND DISCUSSION

This section focuses on the effects that take place in the flowfield structure inside the gaps due to variations on the gap L/H ratio. In order to present the problem coherently, it is necessary to repeat the analysis of previous publication (Paolicchi and Santos, 2009) to some extent. In doing so, this section will present the behavior of the velocity field within the gaps for L/H ratio from 1 to 1/4.

Tangential velocity profiles inside the gaps are demonstrated in Fig. 3 for three sections parameterized by the L/H ratio. In this set of plots, the tangential velocity u is normalized by the freestream velocity U_∞ , the dimensionless height Y corresponds to the height y normalized by the freestream mean free path λ_∞ , and X'_L represents the distance $(x - L_u - L/2)$ normalized by the gap length L . According to this set of plots, the behavior of the tangential velocity profiles is similar for the sections shown. The tangential velocity ratio is zero at the bottom of the gaps, it becomes negative for the range $-7 < Y < -1$, and then it is positive for $Y > -1$.

Normal velocity profiles inside the gaps are displayed in Fig. 4 for three sections as a function of the streamwise distance and parameterized by the L/H ratio. In this set of diagrams, the normal velocity v is normalized by the freestream velocity U_∞ , and the three sections correspond to the transversal sections y normalized by the gap height H . According to these plots, near the gap backward face, $X'_L \approx -0.4$, the normal velocity ratio profiles present positive values, meaning that the flow is moving upward. Conversely, at the vicinity of the gap forward face, $X'_L \approx 0.4$, the normal velocity ratio profiles present negative values, indicating that the flow is moving downward. Therefore, based on these two opposite behaviors for the normal velocity ratio, it may be inferred in passing that there is a region of a clockwise circulating flow. In addition, of particular interest is the behavior of the normal velocity profiles for the $L/H < 1/2$ cases near to the bottom surface of the gaps, i.e., for section $Y_H = -0.75$. It is quite apparent that the v -velocity component is zero, indicating that

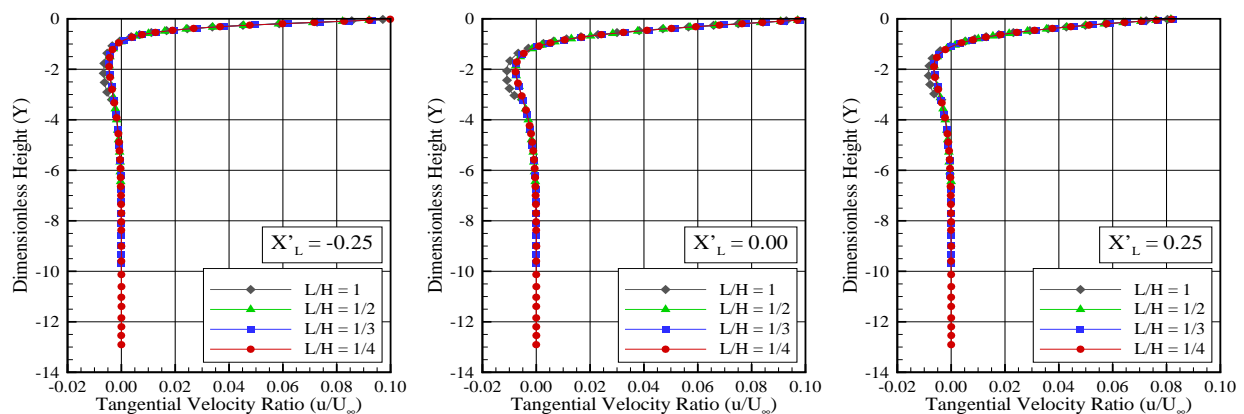


Figure 3. Distribution of tangential velocity (u/U_∞) inside the gaps for three longitudinal sections as a function of the L/H ratio.

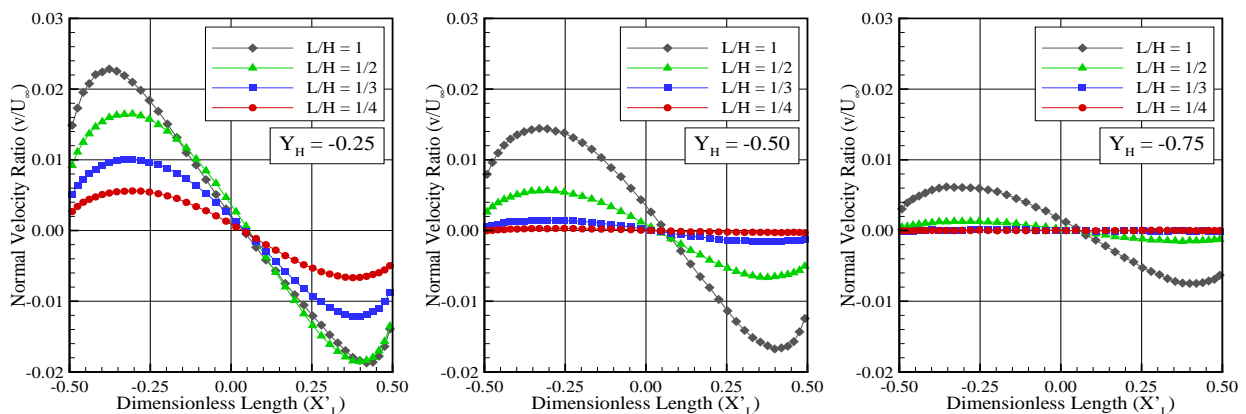


Figure 4. Distribution of normal velocity (v/U_∞) inside the gaps for three transversal sections as a function of the L/H ratio.

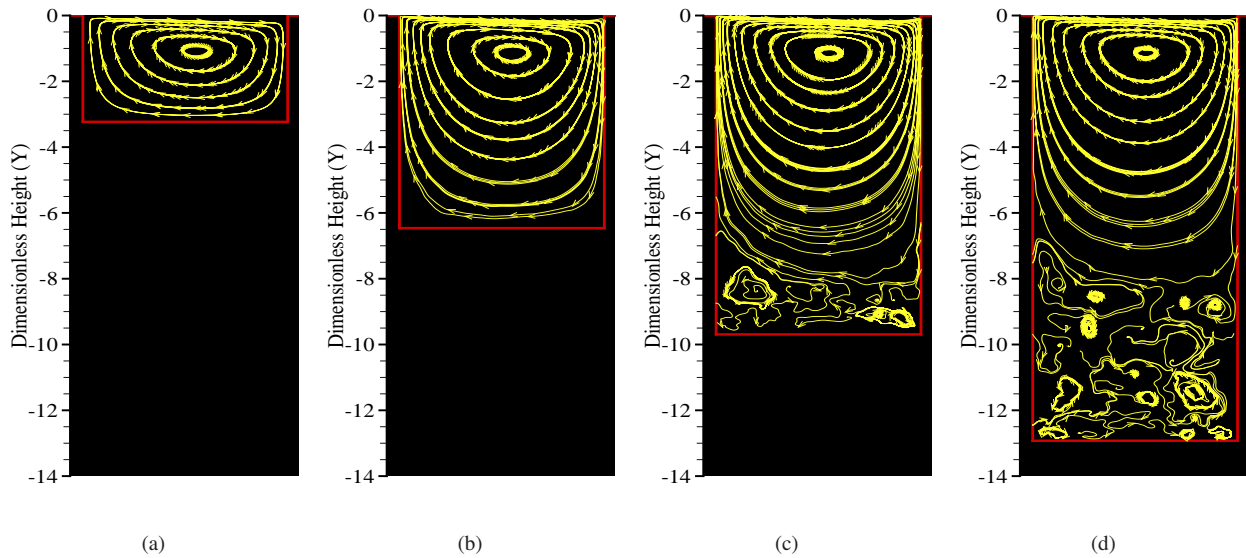


Figure 5. Distribution of streamline traces for L/H ratio of (a) 1, (b) 1/2, (c) 1/3 and (d) 1/4.

there are no recirculation regions at the vicinity of the gap floor for these cases.

At this point, it is worth taking a closer look at the recirculation region. In this manner, streamline traces inside the gaps are depicted in Fig. 5 as a function of the L/H ratio. Based on Fig. 5, it is clearly noticed that the flow within the gaps is characterized by a primary vortex system. For the $L/H = 1$ and $1/2$ cases, it is noteworthy that the recirculation region fills the entire gaps. Conversely, for the $L/H = 1/3$ and $1/4$ cases, the recirculation region does not fill the entire gaps. In addition, the external stream does not reattach at the bottom surface of the gaps.

Still referring to Fig. 5, it is clearly noticed that the gap flow topology observed here in a rarefied environment differs from that usually observed in the continuum flow regime, as shown in Fig. 2(a). Of particular interest is the flow behavior for $L/H = 1/3$ and $1/4$, where the flow exhibits an irregular or chaotic structural motion in the second half part of the gaps, more precisely for $Y < -7$.

In an attempt to find out the formation of a second recirculation region, two new cases were investigated. The previous gap length L of 3 mm was increased to 4 and 5 mm. Nevertheless, the L/H ratio was kept to $1/4$. In principle, by

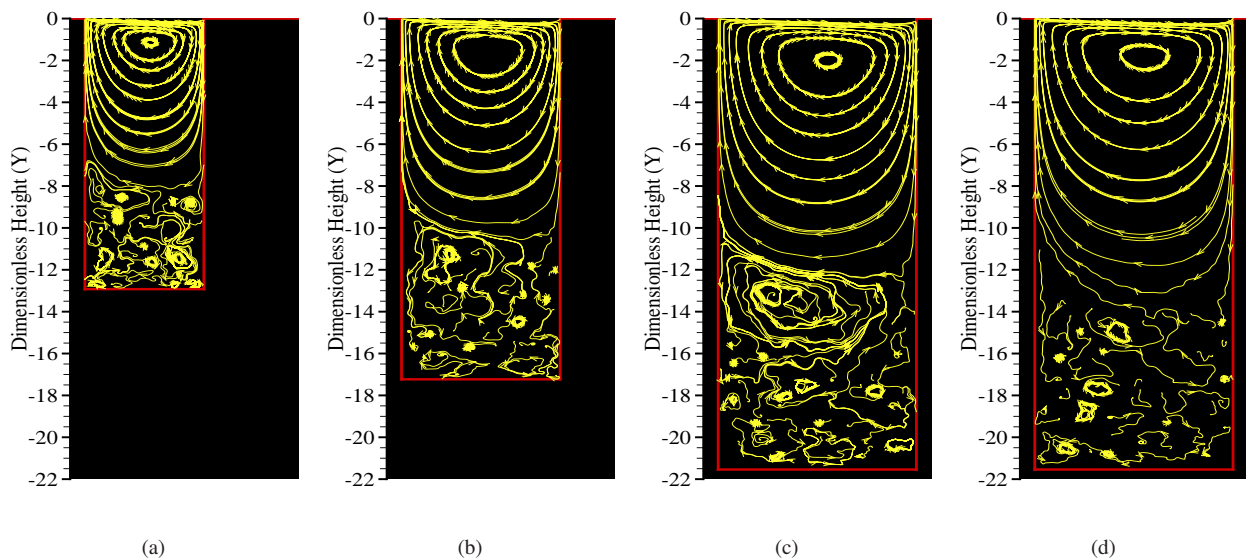


Figure 6. Distribution of streamline traces for the $L/H = 1/4$ case with gap length L of (a) 3 mm, (b) 4 mm, (c) 5 mm and (d) 5 mm with wall temperature of 1760 K.

increasing the gap length L and, consequently, by increasing the gap height H in order to keep $L/H = 1/4$, the Knudsen number decreases, and it is expected that the flow structure inside the gaps changes to or approaches to that observed in the continuum flow.

Streamline traces inside this new series of gaps are demonstrated in Fig. 6. In this set of plots, Figs. 6(a), 6(b) and 6(c) correspond to gap length L of 3, 4, and 5 mm, respectively. According to this set of plots, the flow structure for the $L = 4$ mm case is similar to that for the $L = 3$ mm case. On the other hand, for the $L = 5$ mm case, the flow structure indicates the possible formation of a vortex pattern immediately below of the primary one. Nevertheless, the streamlines do not show clearly a recirculation region on a sufficient large scale like that of the primary vortex.

At this point it is worth taking a closer look at these results. According to Figs. 3 and 4, for the $L/H = 1/4$ case, the macroscopic flow velocity is essentially zero for sections defined by $Y < -7$ or $Y_H \leq -0.50$. As a result, molecules have only their thermal velocities or the random velocities in this part of the gap. In this scenario, if the wall temperature is increased, molecules are reflected from the gap surface with more energy. In addition, the translational energy of the molecules increases and, consequently, the translational temperature would increase. Moreover, by increasing the temperature, the viscosity increases. In this fashion, it is expected that the second “recirculation region”, shown in Fig. 6(c), disappear with viscosity rise. With this perspective in mind, the flowfield structure inside the gap, defined by the $L/H = 1/4$ case with $L = 5$ mm, was investigated again, but this time with wall temperature $T_w = 1760$ K. It should be remarked that this value is twice of the previous cases investigated. In doing so, Fig. 6(d) illustrates the streamline traces for this particular case. As indeed is clear from this figure, the possible second “recirculation region” is completely dissipated.

By the time being, it proves convenient to demonstrate the behavior of viscosity, density and translational temperature inside the gaps. In this manner, Figs. 7, 8, and 9 display, respectively, the viscosity, density, and translational temperature

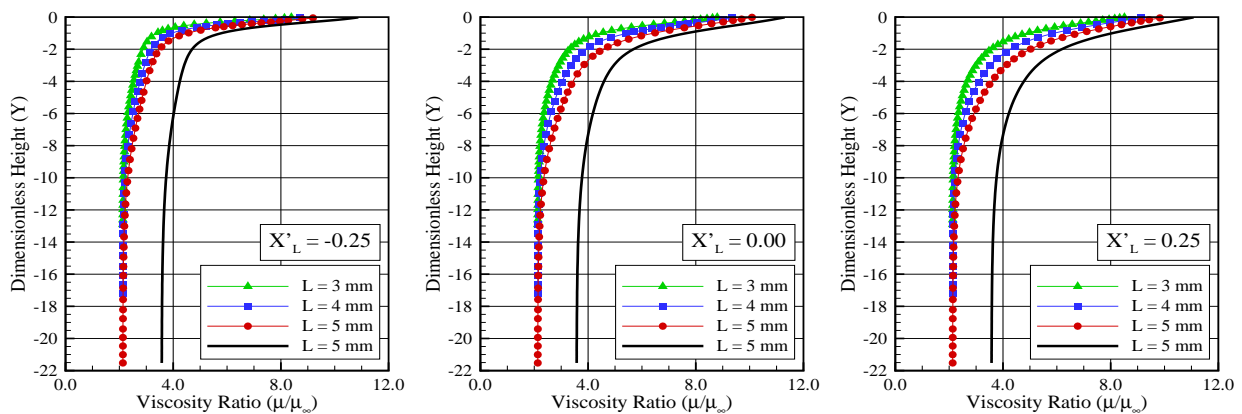


Figure 7. Distribution of viscosity ratio (μ/μ_∞) profiles for three transversal sections inside the gaps as a function of the gap length L .

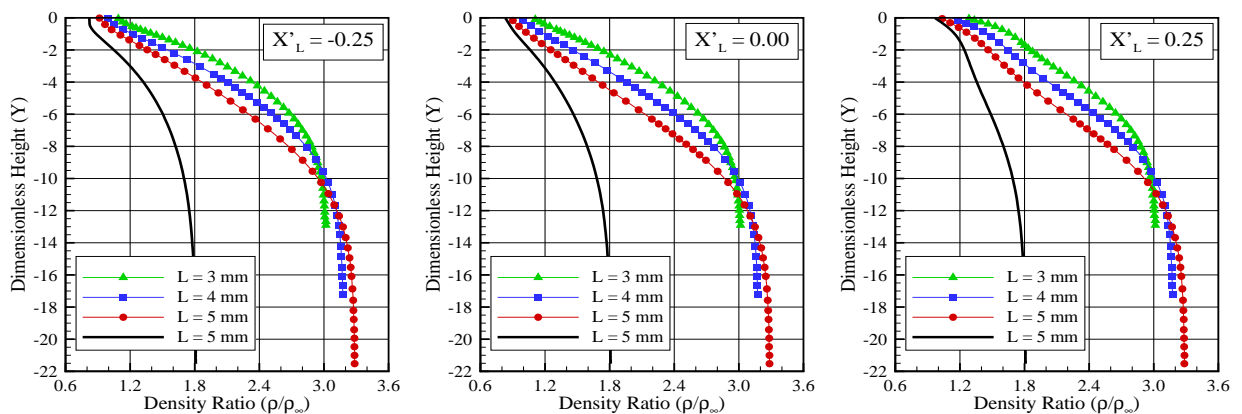


Figure 8. Distribution of density ratio (ρ/ρ_∞) profiles for three transversal sections inside the gaps as a function of the gap length L .

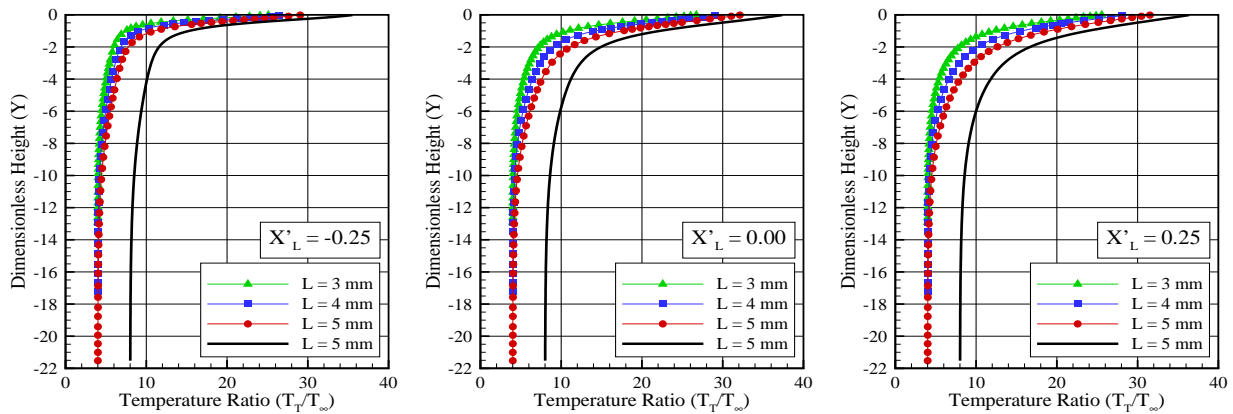


Figure 9. Distribution of translational temperature ratio (T_T/T_∞) profiles for three transversal sections inside the gaps as a function of the gap length L .

profiles for sections X'_L of -0.025, 0.00, and 0.25. In this group of plots, viscosity μ , density ρ , and translational temperature T_T were normalized by their respective freestream values, i.e., μ_∞ , ρ_∞ , and T_∞ . In addition, symbols correspond to the $L/H = 1/4$ case with length L of 3, 4, and 5 mm, and the solid line corresponds to the particular case $L = 5$ mm with wall temperature T_w of 1760 K.

Looking first at Fig. 7, it is clearly noticed that the viscosity ratio presents high values at the top of the gaps. After that, the viscosity ratio drops off up to the center of the gaps, $Y \approx -14$. Afterwards, it presents a constant value up to the bottom of the gaps, where μ is around twice of the freestream viscosity μ_∞ . It is also noticed that the viscosity ratio increased by increasing the wall temperature, as expected.

Referring to Fig. 8, it is observed that the density ratio is in contrast to the viscosity ratio in the sense that density ratio presents small values at the top of the gaps and high values at the bottom of the gaps. Particular attention is paid to the density ratio for the cases with length L of 4 and 5 mm at the vicinity of the top, for section $X'_L = -0.25$. For these cases, the density ρ is less than the freestream density ρ_∞ , i.e., $\rho/\rho_\infty < 1$. This is an expected behavior since the flow experiences an expansion around the corner of the gap backward face. On the other hand, the flow experiences a compression around the corner of the gap forward face.

Turning next to Fig. 9, it is seen that the translation temperature ratio profiles follow the same trend as that presented by viscosity ratio. This is an expected behavior in the sense that, for gases, $\mu \sim T^\omega$, where the exponent ω , defined as the index viscosity, is tabulated in Tab. 2.

In order to gain some insight into the gap flowfield physics, a brief consideration of the important parameters involved is in order. It is usually accepted without question that length and time scales of molecular motions and turbulence are widely separated, i.e., the smallest turbulent scales are normally very much larger than molecular scales. In this fashion, the ratio between the molecular mean free path λ and the Kolmogorov dissipative scale of turbulence l_D is as follows (Tennekes and Lumley, 1970):

$$\lambda/l_d \propto \frac{M}{(Re)^{1/4}} \propto Kn(Re)^{3/4} \propto (M)^{3/4}(Kn)^{1/4} \quad (1)$$

where M , Re , and Kn are Mach, Reynolds and Knudsen numbers, respectively, and the relation $Re \propto M/Kn$ has been taken into account.

On examining Eq.(1), it is very encouraging to observe that, under rarefied hypersonic conditions, for instance, $Kn \approx 0.001$ and $M \approx 10$, λ and l_D are of the same order of magnitude. For the present account, for the $L/H = 1/4$ case with length $L = 5$ mm, $M_\infty = 25$ and $Kn_H = 0.0464$, and Eq.(1) yields $\lambda/l_D \propto 5.3$. Therefore, λ/l_D is of order 1. Of course, care must be taken to these estimates since there might be sizable factors of order unit. As a result, these considerations should not be ignored when considering high Mach number flows. This is a complete unexplored area and is certainly worth more attention.

8. CONCLUDING REMARKS

A rarefied hypersonic flow on gaps have been performed by using the Direct Simulation Monte Carlo method. The calculations provided information concerning the nature of the flowfield structure inside the gaps defined by a Length-to-Depth (L/H) ratio of 1/4 with a representative range of length L . The length L ranged from 3 to 5 mm, which

corresponded Knudsen numbers in the transition flow regime.

It was found that the flow topology inside the gaps presented only one recirculation region for the range of the conditions investigated in the present account. This is in contrast to the flowfield structure observed for gaps in the continuum flow regime, where the number of vortices is estimated by the H/L ratio.

9. ACKNOWLEDGEMENTS

The authors would like to thank the financial support provided by CNPq (Conselho Nacional de Desenvolvimento Científico e Tecnológico) under Grant No. 473267/2008-0.

10. REFERENCES

- Alexander, F. J., Garcia, A. L., and Alder, B. J., 1998. "Cell Size Dependence of Transport Coefficient in Stochastic Particle Algorithms", *Physics of Fluids*, Vol. 10, pp. 1540–1542.
- Alexander, F. J., Garcia, A. L., and Alder, B. J., 2000. "Erratum: Cell Size Dependence of Transport Coefficient in Stochastic Particle Algorithms", *Physics of Fluids*, Vol. 12, pp. 731–731.
- Bertin, J. J., and Goodrich, W. D., 1980. "Aerodynamic Heating for Gaps in Laminar and Transitional Boundary Layers", 18th AIAA Aerospace Sciences Meeting and Exhibit, AIAA Paper 80-0287, Pasadena, CA, USA, January 14–16.
- Bird, G. A., 1981. "Monte Carlo Simulation in an Engineering Context", In Fisher, S. S., ed., *Progress in Astronautics and Aeronautics: Rarefied gas Dynamics*, Vol. 74, part I, AIAA New York, pp. 239–255.
- Bird, G. A., 1989. "Perception of Numerical Method in Rarefied Gasdynamics", In Muntz, E. P., Weaver, D. P., and Capbell, D. H., eds., *Rarefied Gas Dynamics: Theoretical and Computational Techniques*, Vol. 118, *Progress in Astronautics and Aeronautics*, AIAA, New York, pp. 374–395.
- Bird, G. A., 1994. *Molecular Gas Dynamics and the Direct Simulation of Gas Flows*, Oxford University Press.
- Borgnakke, C. and Larsen, P. S., 1975. "Statistical Collision Model for Monte Carlo Simulation of Polyatomic Gas Mixture", *Journal of Computational Physics*, Vol. 18, No. 4, pp. 405–420.
- Everhart, J. L., Alter, S. J., Merski, N. R., and Wood, W. A., and Prabhu, R. K., 2006. "Pressure Gradient Effects on Hypersonic Cavity Flow Heating", 44th AIAA Aerospace Sciences Meeting and Exhibit, AIAA Paper 2006-0185, Reno, NV.
- Garcia, A. L., and Wagner, W., 2000. "Time Step Truncation Error in Direct Simulation Monte Carlo", *Physics of Fluids*, Vol. 12, pp. 2621–2633.
- Hadjiconstantinou, N. G., 2000. "Analysis of Discretization in the Direct Simulation Monte Carlo", *Physics of Fluids*, Vol. 12, pp. 2634–2638.
- Harvey, J. K., 1986. "Direct Simulation Monte Carlo Method and Comparison with Experiment", *Rarefied Gas Dynamics: Thermophysical Aspect of Re-entry Flows*, Eds. J. N. Moss and C. D. Scott, Vol. 103, pp. 25–43, *Progress in Astronautics and Aeronautics*, AIAA, Washington, DC.
- Harvey, J. K., and Gallis, M. A., 2000. "Review of Code Validation Studies in High-Speed Low-Density Flows", *Journal of Spacecraft and Rockets*, Vol. 37, pp. 8–20.
- Harvey, J. K., and Gallis, M. A., 2003. "A Review of a Validation Exercise on the Use of the DSMC Method to Compute Viscous/Inviscid Interactions in Hypersonic Flow", AIAA Paper 2003-3643.
- Hinderks, M., Radespiel, R., and Gülhan, A., 2004. "Simulation of Hypersonic Gap Flow with Consideration of Fluid Structure Interaction", 34th AIAA Fluid Dynamics Conference and Exhibit, AIAA Paper 2004-2238, Portland, OR.
- Hinderks, M., and Radespiel, R., 2006. "Investigation of Hypersonic Gap Flow of a Reentry Nosecap with Consideration of Fluid structure Interaction", 44th AIAA Aerospace Sciences Meeting and Exhibit, AIAA Paper 2006-0188, Reno, NV, USA, January 9–12, 2006.
- Holden, M. S. and Wadhams, T. P., 2003. "A Review of Experimental Studies for DSMC and Navier-Stokes Code Validation in Laminar Regions of Shock/Shock and Shock/Boundary Layer Interaction Including Real Gas Effects in Hypersonic Flows", AIAA Paper 2003-3641.
- Paolicchi, L. T. L. C., and Santos, W. F. N., 2009. "Direct Simulation Calculations of Rarefied Hypersonic Gap Flow", 3rd Southern Conference on Computational Modeling, Rio Grande, RS, Nov. 23–25 Nov.
- Paolicchi, L. T. L. C., and Santos, W. F. N., 2010. "Heat Transfer and Pressure Distribution in a Rarefied Hypersonic Gap Flow", XIII Encontro de Modelagem Computacional, Nova Friburgo, RJ, Nov. 3–5 Nov.
- Paolicchi, L. T. L. C., 2010. *Computational Analysis of Gap Effects on the Surface of Reentry Space Vehicles. MS Thesis*, INPE (National Institute for Space Research), Brazil.
- Petley, D. H., Smith, D. M., Edwards, C. L. W., Carlson, A. B., and Hamilton II, H. H., 1984. "Surface Step Induced Gap Heating in the Shuttle Thermal Protection System", *Journal of Spacecraft and Rockets*, Vol. 11, No. 2, pp. 156–161.
- Pitts, W. C., and Murbach, M. S., 1982. "Flight Measurements of Tile Gap Heating on the Space Shuttle", AIAA/ASME 3rd Joint Thermophysics, Fluids, Plasma and Heat Transfer Conference, AIAA Paper 82-0840, St. Louis, MO.
- Scott, C. D., and Maraia, R. J., 1979. "Gap Heating with Pressure Gradients", 14th AIAA Thermophysics Conference, AIAA Paper 79-1043, Orlando, FL, USA, June 4–6, 1979.

- Smith, D. M., Petley, D. N., Edwards, C. L. W., and Patten, A. B., 1983. "An Investigation of Gap Heating Due to Stepped Tiles in Zero Pressure Gradient Regions of the Shuttle Orbiter Thermal Protection System", 21st AIAA Aerospace Sciences Meeting and Exhibit, AIAA Paper 83-0120, Reno, NV, USA, January 10–13.
- Tennekes, H., and Lumley, J. L., 1970. A First Course in Turbulence, The MIT Press, Massachusetts.
- Vharbonnier, J., and Boerrigter, H., 1993. "Contribution to the Study of Gap Induced Boundary Layer Transition in Hypersonic Flow", AIAA/DGLR 5th International Aerospace Planes and Hypersonics Technologies Conference, AIAA Paper 93-5111, Munich, Germany.

11. Responsibility notice

The authors are the only responsible for the printed material included in this paper.